Bull. Mater. Sci., Vol. 39, No. 1, February 2016, pp. 19–26. © Indian Academy of Sciences.

Hydrothermal growth of ZnO nanoflowers and their photocatalyst application

JINCHENG FAN[1,*], TENGFEI LI[1] and HANG HENG[2,3]

[1]School of Materials Science and Engineering, Anhui University of Technology, Maanshan 243002, China
[2]Center for Analysis and Testing, Nanjing Normal University, Nanjing 210097, China
[3]Department of Physics, Nanjing Normal University, Nanjing 210097, China

MS received 16 January 2015; accepted 9 October 2015

Abstract. **ZnO nanoflowers were prepared by the hydrothermal method and studied by X-ray diffraction, Raman spectroscopy, scanning electron microscopy, transmission electron microscopy, energy-dispersive X-ray spectroscopy and photoluminescence. ZnO nanoflowers with star-like morphology were of pure wurtzite phase. The edges of the petals were composed of assemblies of smaller nanocrystallites. Green and orange emissions in photoluminescence were attributed to O vacancies and O interstitials, respectively. Furthermore, ZnO nanoflowers demonstrated the effective photocatalytic activities, and O vacancies and O interstitials were considered to be the active sites of the ZnO photocatalyst.**

Keywords. **ZnO nanoflowers; luminescence; O defects; photocatalyst.**

1. Introduction

With a wide band gap (3.37 eV) and a large exciton binding energy of 60 meV at room temperature, ZnO has attracted much attention due to its potential applications in electronic and optoelectronic devices [1,2], gas sensors [3–5], field-emission devices [6–8], solar cells [9–11] and photocatalysts [12–14]. Besides TiO_2, ZnO is considered as a promising material for purification and disinfection of water and air owing to its nontoxic nature, low cost and high reactivity [15–17]. Under the ultraviolet (UV) irradiation, the electrons in ZnO are excited from the valence band to the conduction band, and the excited electrons and the corresponding holes can activate the surrounding chemical species and then promote the chemical reactions. Therefore, ZnO materials can be used as photocatalyst. Various ZnO nanomaterials, such as ZnO nanowires, nanotubes, nanocrystals, have been widely studied as the photocatalyst because of larger specific surface-to-volume area, which exhibit excellent photocatalytic behaviours [18–25]. Currently, the researchers have developed many different approaches to fabricate ZnO nanomaterials, among which hydrothermal growth of ZnO nanostructures is one of the most widely explored methods. The hydrothermal method can present the good productivity without using any rigorous conditions or sophisticated instrumentation [25–27]. ZnO nanomaterials with a variety of new morphologies have been fabricated by the hydrothermal method [25,27].

In this paper, the fabrication of ZnO nanoflowers on Si substrate by the hydrothermal method and their photocatalyst application was reported. The crystal structure and optical properties of ZnO nanoflowers were characterized and the formation mechanism was discussed. Specially, the photocatalytic performances of ZnO nanoflowers were investigated, exhibiting the effective photocatalytic behaviours for the degradation of dyes. Photocatalytic mechanism was discussed and O vacancies and O interstitials were considered to be the active sites of the ZnO photocatalyst.

2. Experiment

2.1 *Fabrication of ZnO seeds*

For the preparation of ZnO seeds, the typical easy process is summarized as follows: 0.2 g of $Zn(CH_3COO)_2{\cdot}2H_2O$ was dissolved into 50 ml *N*,*N*-dimethylformamide (C_3H_7NO), and was magnetically stirred for 20 min at room temperature, vigorously, and then the solution was transferred to incubator and remained at 90°C for 4 h, and then was cooled to room temperature. Finally, the solution was composed of the clear solution (up) and white deposited gel solution (down). The clear solution was removed and the white sol solution was remained to prepare ZnO seeds for the fabrication of ZnO nanoflowers.

2.2 *Synthesis of ZnO nanoflowers*

Before the growth of ZnO nanoflowers, Si was cleaned in acetone, ethanol and deionized (DI) water, and dried in air

*Author for correspondence (fanjincheng2009@163.com)

Figure 1. Schematic process for fabricating ZnO nanoflowers.

to remove the contaminants on the surface of Si. Then, Si substrate was coated with the white sol solution prepared in above step by dropping and dried in air. After that, the coated Si was rinsed in acetone, ethanol and DI water to remove the organic residue and ZnO seeds were remained on the surface of Si. Then, the seeded Si was placed in an aqueous solution (160 ml, pH = 11) containing 0.3 g $Zn(NO_3)_2{\cdot}6H_2O$ and 0.1 g NaOH at 70 or 80°C for 70 min under continuous magnetic stirring. After the reaction, ZnO nanoflowers were grown on Si substrates. Finally, the samples were rinsed in DI water to remove any residual salt and dried in air. The samples grown at 70 and 80°C were marked Sample A and Sample B, respectively. The process is schematically shown in figure 1. Obviously, the chemicals used in the experiment show some advantages, such as low cost and less hazardous. The growth occurs at a relatively low temperature, there is no need for the use of metal catalysts. It is believed that the hydrothermal method with the chemicals is a very powerful and versatile technique to fabricate ZnO nanomaterials.

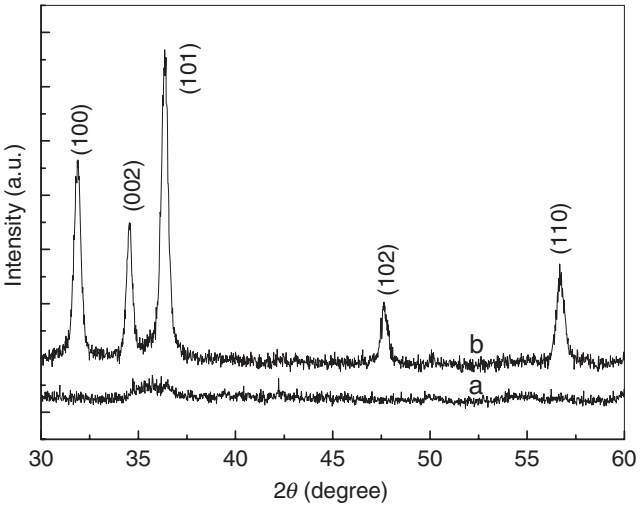

Figure 2. XRD patterns of the ZnO nanoflowers grown at (**a**) 70 and (**b**) 80°C.

2.3 *Characterization*

The crystal structure and morphologies of ZnO nanoflowers were performed by X-ray diffraction diffractometer (XRD, BrukerD8, CuKα, $\lambda = 0.15405$ nm), Raman spectroscopy (Jobin Yvon HR800UV, $\lambda = 514$ nm), scanning electron microscopy (SEM, FEI Nova NanoSEM 430), and transmission electron microscope (TEM, JEM-2100F). The element compositions of the samples were characterized by an energy-dispersive X-ray spectrometer (EDS, Oxford Instruments). Photoluminescence (PL) was measured with the 325 nm He–Cd laser as an optical excitation. All measurements were carried out at room temperature. To evaluate the photocatalytic activities of ZnO nanoflowers, ZnO nanoflowers/Si (1.5 cm × 1.5 cm) was immersed into 25 ml Rhodamine B (RhB) aqueous solution (5 mg l^{-1}) and irradiated by 50 W UV light. Then, 2.5 ml reaction samples were withdrawn periodically for UV–vis analysis. The degradation efficiency was evaluated by the equation: $\eta = (1-C/C_0)$, where C and C_0 are the concentrations of RhB after and before UV irradiation, respectively. C/C_0 is calculated by A/A_0, because the concentration of RhB is linearly proportion to absorption (A).

3. Results and discussion

Figure 2 displays the XRD patterns of ZnO nanoflowers. For the ZnO nanoflowers grown at 70°C, only a broad peak between 34.5° and 36.6° was observed (figure 2a), indicating that the poor crystallinity of ZnO nanoflowers grown at lower temperature (70°C). However, in the XRD pattern of ZnO nanoflowers grown at 80°C (figure 2b), three distinct peaks at 31.9°, 34.5° and 36.4° were detected, corresponding to (100), (002) and (101) ZnO crystal planes, respectively. It could be assigned as hexagonal ZnO phase denoting P63mc space group (JCPDS no. 361451). The lattice constants were calculated as $a = 3.249$ Å, $c = 5.206$ Å, corresponding to the wurtzite structure of ZnO. No impurity peaks, such as $Zn(OH)_2$, were observed in XRD pattern of ZnO nanoflowers, indicating the formation of a pure ZnO phase.

Raman spectrum can be used to investigate the crystal quality, structural defects and disorders of materials. The wurtzite structure of ZnO belongs to the space group C_{6v}^4 (P63mc). One primitive cell includes two formula units and all of the atoms occupy 2b sites of symmetry C3v. Group theory predicted, at the Γ point of the Brillouin zone, there is an existence of following optic modes: $\Gamma = A_1 + 2B_1 + E_1 + 2E_2$, and the A_1, E_1 and E_2 modes are Raman actives [28–30]. Figure 3 shows the Raman spectra of ZnO nanoflowers. For ZnO nanoflower grown at 70°C, a weak peak at 432 cm^{-1} was detected, while a remarkable peak at 438 cm^{-1} was observed for ZnO nanoflower grown at 80°C. Compared with the Raman spectra of ZnO crystal, the remark peak could be assigned to the E_2 mode of hexagonal wurtzite phase of ZnO nanoflowers, confirming the good crystallinity quality of ZnO nanoflowers grown at 80°C.

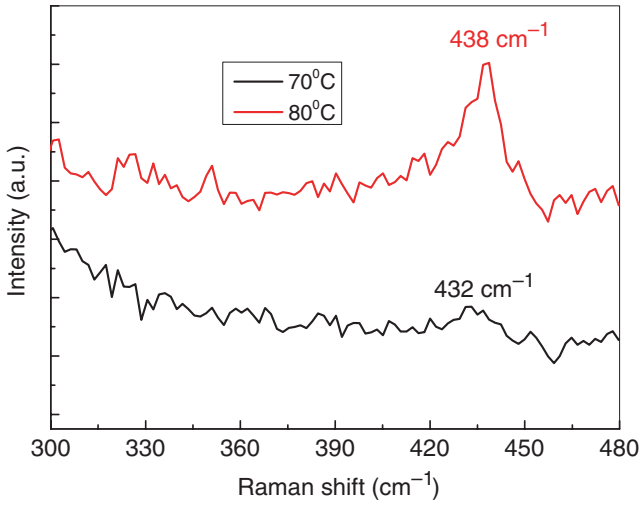

Figure 3. Raman spectra of the ZnO nanoflowers.

Morphological properties of ZnO nanoflowers were investigated by SEM, as illustrated in figure 4. The image of seeded Si surface (figure 4a) displays that the seeds were distributed uniformly and compactly. With 70°C and 70 min, a large mass of quasispherical ZnO nanocrystals and a small amount of ZnO flower embryo were produced (figure 4b). Afterward, ZnO nanoflowers were grown when the growth temperature was increased to 80°C (figure 4c).

The growth process of ZnO nanoflowers could be attributed to the initial precipitation of the $Zn(OH)_2$. The formed $Zn(OH)_2$ dissolved to a considerable extent in water, forming $Zn(OH)_4^{2-}$ ions. When the concentrations of $Zn(OH)_4^{2-}$ ions exceeded the critical value, ZnO nanoflowers were developed, and the relevant chemical reactions can be written as follows [31]:

$$Zn^{2+} + 2OH^- \rightarrow Zn(OH)_2\downarrow, \quad (1)$$

$$Zn(OH)_2 + 2OH^- \rightarrow Zn(OH)_4^{2-}, \quad (2)$$

$$Zn(OH)_4^{2-} \rightarrow ZnO + H_2O + 2OH^-. \quad (3)$$

Compared to the ZnO precipitate, the $Zn(OH)_2$ precipitate was more soluble, which produced continuously $Zn(OH)_4^{2-}$ ions and ZnO nanoflowers were produced.

Figure 5 shows SEM images of ZnO nanoflowers with the different magnifications. From low and middle magnifications (figure 5a–c), it could be seen that ZnO nanoflowers were distributed on the surface of Si substrate, indicating a large-scale fabrication of ZnO nanoflowers. ZnO nanoflowers exhibited the petals with 200–400 nm in length and 100–200 nm in width (figure 5d).

The morphology of the as-grown ZnO nanoflowers was further characterized by TEM analysis, as shown in figure 6. It could be seen that the shape of ZnO nanoflowers resembled star-like morphology and the edges of ZnO petal were not smooth and were composed of assemblies of smaller nanocrystallites. The corresponding selected area electron diffraction (SAED) pattern also confirmed single crystalline

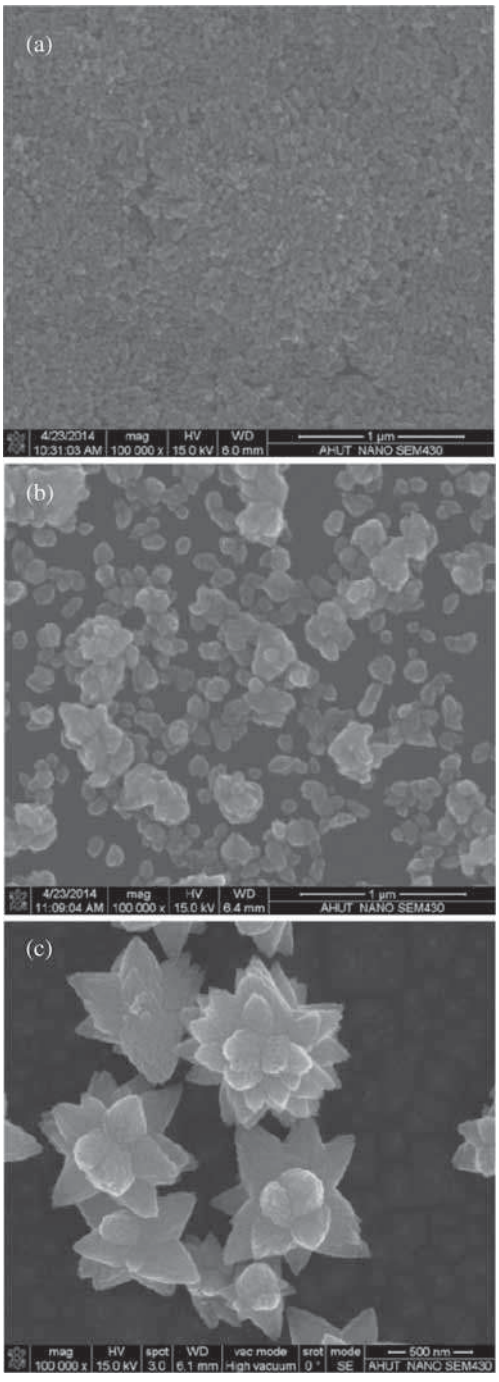

Figure 4. SEM images for (**a**) seeded Si substrate, (**b**) ZnO nanoflowers grown with 70°C and 70 min and (**c**) ZnO nanoflowers grown with 80°C and 70 min.

of ZnO nanoflowers. EDS analysis of ZnO nanoflowers indicated the presence of Zn and O (figure 6c), suggesting the formation of a pure ZnO phase, which was consistent with the XRD result (figure 2). Obviously, Si peak could be attributed to Si substrate.

The HR-TEM image of ZnO nanocrystalline at the edge of ZnO petal demonstrated the lattice spacing was around

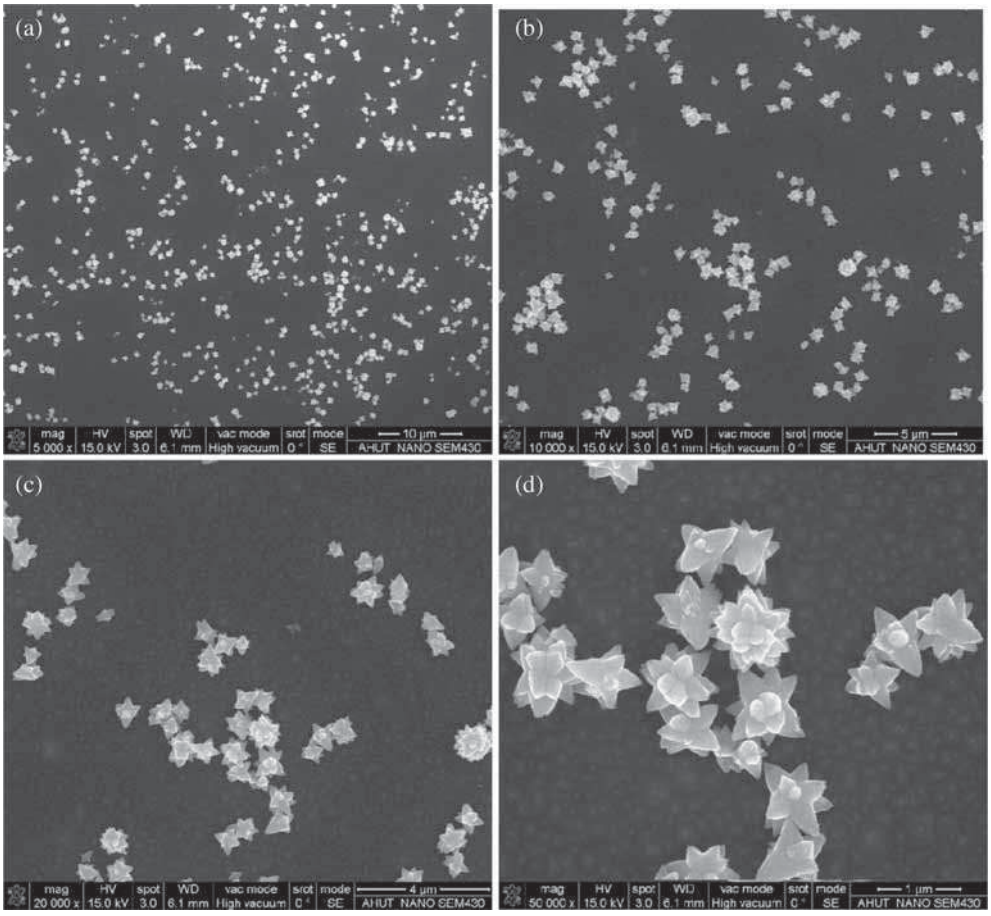

Figure 5. FE-SEM images of ZnO nanoflowers with (**a**) low magnification, (**b** and **c**) medium magnification and (**d**) high magnification.

0.25 nm, corresponding to the interspacing of the (002) planes (figure 7) [32–34].

The optical properties of ZnO nanoflowers were investigated by PL at room temperature. Figure 8 shows PL spectra of ZnO nanoflowers prepared with various temperatures. The typical emissions of narrow violet (∼380 nm) and broad visible bands were observed. The UV emission could be attributed to the radiative annihilation of excitons origined from the exciton–exciton collisions in ZnO. The UV luminescence from ZnO nanoflowers was enhanced with the increase of the growth temperature, which indicated the better crystallinity of ZnO nanoflowers prepared at higher temperature (80°C) and was consisted with the results obtained from SEM images (figure 4). At lower growth temperature (70°C), ZnO nanoflowers could not be developed fully due to the lower energy, resulting in the poor crystallinity. The result was also confirmed by weak UV luminescence (figure 8a and b).

As shown in figure 8, both of samples grown at 70 and 80°C exhibited broad visible luminescences. Obviously, the visible luminescence intensity of the sample at 70°C was stronger than that of sample at 80°C, which indicated more defects in the sample grown at lower temperature, because the luminescence in the visible region was commonly assigned to the deep-level defects in ZnO, such as vacancies and interstitials of oxygen and zinc, but the origin of the visible emissions was still highly controversial [35,36]. The native defects with different energy levels in ZnO have been studied widely by the researchers [37–39]. O vacancy (V_O) and O interstitial (O_i) are known to be the most common defects in ZnO materials. They serve as the radiative centres in luminescence processes and play the significant roles to determine the visible luminescence for ZnO materials. Specially, a O vacancy has three possible charge states: the neutral oxygen vacancy (V_O^x), the singly ionized oxygen vacancy (V_O^+) and the doubly ionized oxygen vacancy (V_O^{++}). The different charge states of oxygen vacancies occupy different energy levels in the ZnO band-gap, which are responsible for the visible luminescence the different wavelengths [40,41]. Yellow, green and blue luminescences from ZnO could be attributed to V_O^{++}, V_O^+ and V_O^x, respectively [42]. In our experiments, Gaussian fitting was used to study the PL spectra of ZnO nanoflowers, as shown in figure 8b and c. The fitting peaks are summarized in table 1. PL spectra of ZnO nanoflowers demonstrated four fitting peaks at ∼380 (UV), ∼550 (green), ∼620 (orange) and ∼760 nm (near-infrared, NIR), respectively. The green emission could be considered to correspond to V_O defects, due to the electron transition

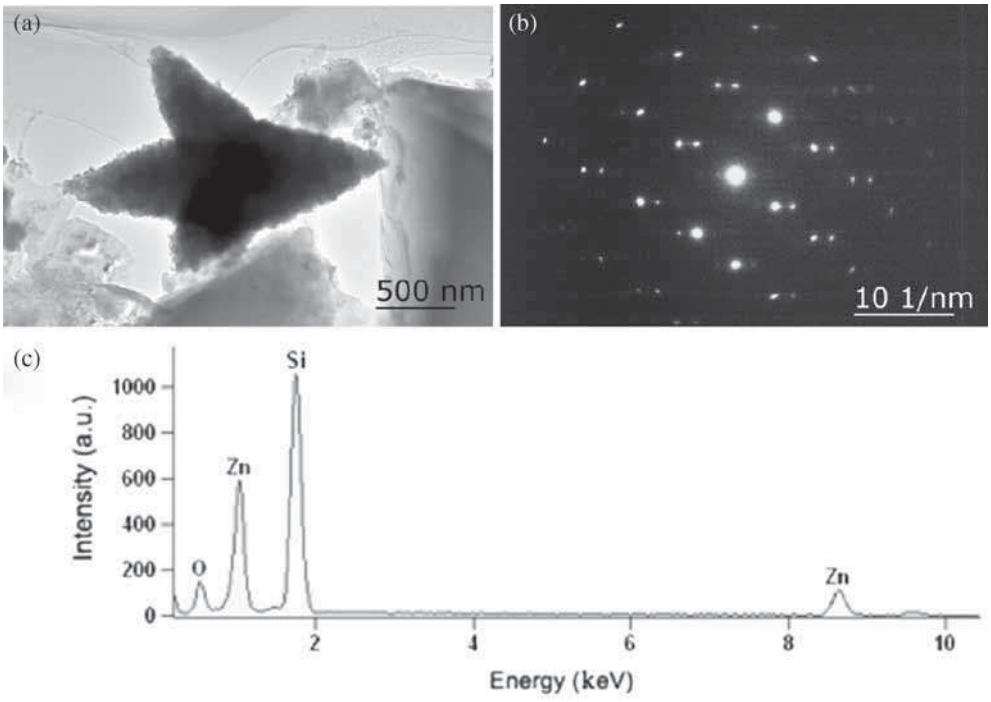

Figure 6. (**a**) TEM image of flower-like ZnO nanostructure, (**b**) SAED pattern of flower-like ZnO nano-structures and (**c**) EDS spectrum of ZnO nanoflowers.

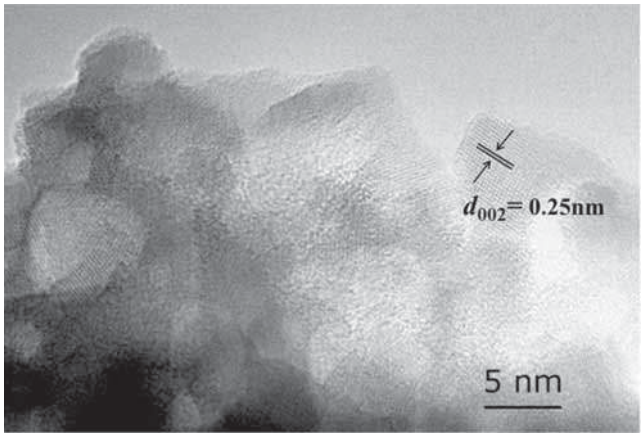

Figure 7. Typical HR-TEM image of the edge at the petal of ZnO nanoflowers.

from the V_O centres to the valence band edge. In the PL spectra of ZnO nanoflowers, orange emission centred ∼620 nm was observed. Actually, orange emission has been less commonly detected than green emission, and could be assigned to O_i defects [43–45].

NIR luminescence at ∼750 nm was detected in the PL spectra. It was also noted that its intensity was enhanced for ZnO nanoflowers with a strong UV luminescence. In the case, the NIR luminescence in our experiments could be assigned to the second-order diffraction of UV luminescence. Generally, NIR luminescence in ZnO PL spectrum is contributed to the second-order diffraction of UV luminescence. However, some researchers reported that the NIR luminescence at about 750 nm was attributed to the oxygen vacancies in ZnO materials [46]. In our experiments, ZnO nanoflowers with better crystalline and lower emission in visible region exhibited a stronger NIR luminescence. The phenomenon was not in agreement with the reports that NIR luminescence originated from O vacancies. Actually, the NIR luminescence at ∼750 nm was often observed in PL spectra with a strong UV luminescence when PL spectra was measured for ZnO materials, including ZnO nanopowders, nanorods and nanoflowers. Therefore, the NIR luminescence in our experiments could be attributed to the second-order diffraction of UV luminescence.

The photocatalytic properties of ZnO nanoflowers were investigated through the photodegradation of RhB aqueous solution under UV light irradiation. Figure 9 shows photocatalytic performances of ZnO nanoflowers. As shown in figure 9a, during the reaction process, the absorption intensity at ∼550 nm of RhB aqueous solution decreased gradually with the irradiation time, indicating the successful reduction of ZnO nanoflowers. After irradiation for 3 h, the degradation efficiency (η) of RhB was found to be about 52%. The plot of $\ln(C/C_0)$ *vs.* time was almost linear (figure 8b inset), which suggested that the photodecomposition reaction following the first-order rate law. Similarly, ZnO nanoflowers grown at 70°C was immersed into RhB solution. After 3 h irradiation, the degradation efficiency (η) of RhB was about 42%. To confirm the photocatalytic properties of ZnO nanoflowers, RhB aqueous solution without ZnO nanoflowers/Si was also irradiated in UV light. Even if after 4 h irradiation, no

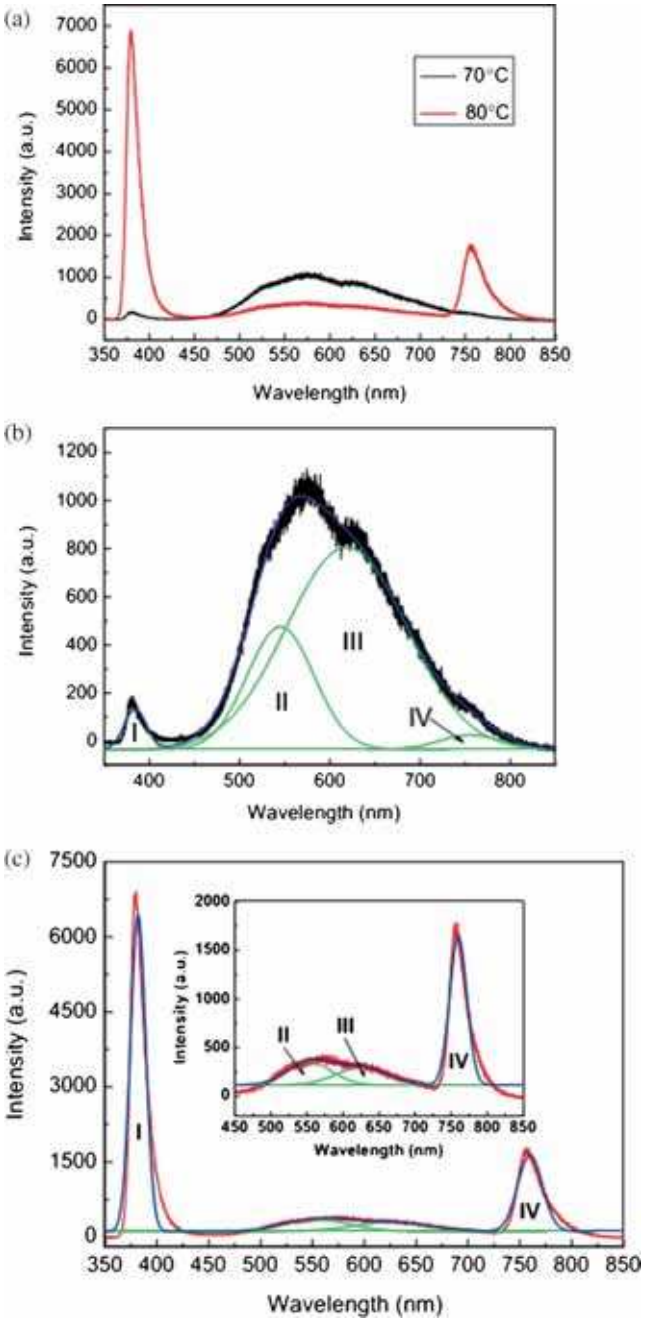

Figure 8. (**a**) PL spectra of the ZnO nanoflowers. (**b**) PL spectrum of ZnO nanoflowers grown at 70°C is deconvoluted by four parts, marked as UV band (I), green band (II), orange band (III) and NIR band (IV); and (**c**) PL spectrum of ZnO nanoflowers grown at 80°C is deconvoluted by four parts, marked as UV band (I), green band (II), orange band (III) and NIR band (IV).

obvious changes for the absorption intensity of RhB aqueous solution were detected in our experiments. The results revealed the degradations of RhB (figure 9) were due to ZnO nanoflowers immersed in it. Therefore, ZnO nanoflowers can work as the effective photocatalysts, which prompts the potential application of our ZnO nanoflowers to the treatment of wastewater.

Table 1. Peak positions of the different luminescence bands from the fitted PL spectra.

	Fitting peak (position, nm)			
Samples	UV	Green	Orange	NIR
A	380	544	616	754
B	381	552	625	758

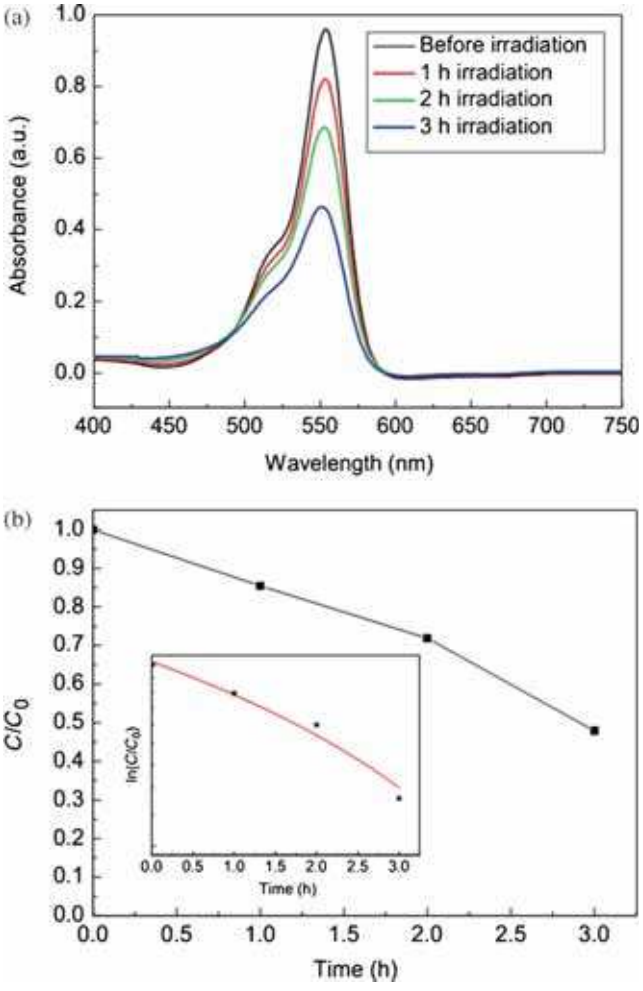

Figure 9. (**a**) Degradation of Rhodamine B with different irradiation times and (**b**) degradation rate of Rhodamine B with ZnO nanoflowers.

Generally, for semiconductor materials, when a photon with an energy of $h\nu$ matches or exceeds the band gap energy (E_g), an electron (e_{cb}^-) in the valence band (VB) can be excited to the conduction band (CB), leaving a hole (h_{vb}^+) in the VB. The photogenerated electrons and holes can recombine and dissipate the input energy as heat, get trapped in metastable surface states, or react with electron donors and electron acceptors adsorbed on the semiconductor surface. With a suitable scavenger or surface defect state, the photoelectron can be trapped by electron acceptors, while the

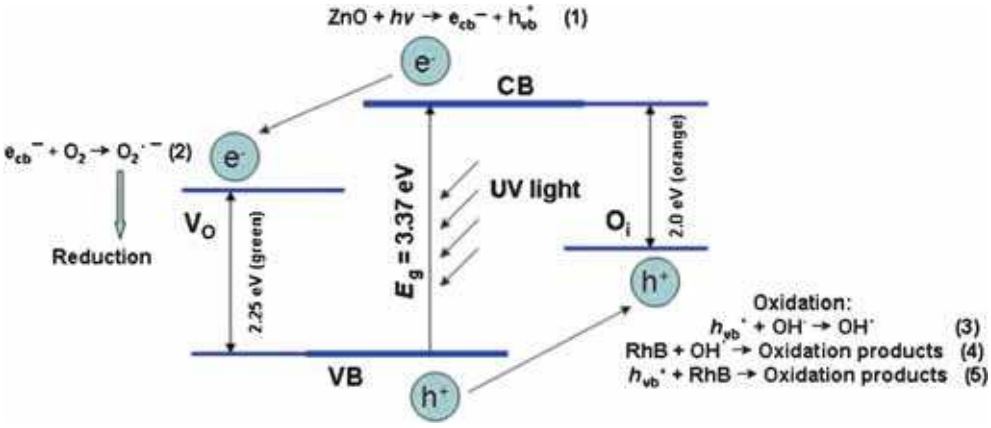

Figure 10. Schematic of the band structure and charge-transfer process, and photocatalytic reaction process of ZnO nanoflowers.

photoinduced holes can be easily trapped by electronic donors. Therefore, photoelectrons and holes restrain the recombination, which results in subsequent redox reactions [14,47–49]. Figure 10 shows schematically the band structure, charge-transfer process and photocatalytic reaction process of ZnO nanoflowers. For ZnO nanoflowers in the redox reactions, the oxygen vacancies served as the electron acceptors and prevented the recombination of e_{cb}^- and h_{vb}^+, while OH^- in the RhB aqueous solution acted as the hole capturing centers and prevented the recombination of photoelectrons and holes. Therefore, ZnO nanoflowers exhibited the effective photocatalystic behaviours and V_O and O_i defects could be considered to be the active sites of ZnO photocatalyst.

4. Conclusions

ZnO nanoflowers were fabricated by the hydrothermal method. The XRD pattern and EDS spectrum elucidated ZnO nanoflowers grown at 80°C were pure wurtzite phase with good crystallinity quality. The length and width of flower petal were about 200–400 and 100–200 nm, respectively. Raman spectrum indicated good crystalline quality of ZnO nanoflowers. TEM and HR-TEM images revealed the edges of ZnO flowers were composed of assemblies of smaller nanocrystallites. PL spectra of ZnO nanoflowers exhibited UV, broad visible and NIR luminescences. UV emission was due to the exciton–exciton collisions, while visible and NIR luminescences were assigned to O defects (V_O and O_i) and the second-order diffraction of UV luminescence, respectively. Furthermore, in our experiments, ZnO nanoflowers demonstrated the effective photocatalytic activities, and ZnO nanoflowers grown at 80°C demonstrated higher degradation efficiency than that of ZnO nanoflowers grown at 70°C. Oxygen vacancies and oxygen interstitials were considered to be the active sites of the ZnO photocatalyst. These results promise a potential application of ZnO nanoflowers in the treatment of wastewater.

Acknowledgement

This work was supported by the Talent Plan at Anhui University of Technology.

References

[1] Janotti A and Van de Walle C G 2009 *Rep. Prog. Phys.* **72** 126501

[2] Litton C W, Reynolds D C and Collins T C (Ed) 2011 *Zinc oxide materials for electronic and optoelectronic device application* (John Wiley & Sons Ltd.)

[3] Wang L W, Kang Y F, Liu X H, Zhang S M, Huang W P and Wang S R 2012 *Sens. Actuators B: Chem.* **162** 237

[4] Mirabbaszadeh K and Mehrabian M 2012 *Phys. Scr.* **85** 035701

[5] Ahn M-W, Park K-S, Heo J-H, Park J-G, Kim D-W, Choi K J, Lee J-H and Hong S-H 2008 *Appl. Phys. Lett.* **93** 263103

[6] Li D, She J C, Xu S Z and Deng S Z 2013 *IEEE Trans. Electr. Dev.* **60** 2924

[7] Zhao Q, Huang C-K, Zhu R, Xu J, Chen L and Yu D P 2011 *Solid State Commun.* **151** 1650

[8] Kuo S-Y and Lin H-I 2014 *Nanoscale Res. Lett.* **9** 70

[9] Zhang M-L, Jin F, Zheng M-L, Liu J, Zhao Z-S and Duan X-M 2014 *RSC Adv.* **4** 10462

[10] Law M, Greene L E, Johnson J C, Saykally R and Yang P D 2005 *Nat. Mater.* **4** 455

[11] Zhang Q F, Dandeneau C S, Zhou X Y and Cao G Z 2009 *Adv. Mater.* **11** 4871

[12] Tian C G, Zhang Q, Wu A P, Jiang M J, Liang Z L, Jiang B J and Fu H G 2012 *Chem. Commun.* **48** 2858

[13] Bai X J, Wang L, Zong R L, Lv Y H, Sun Y Q and Zhu Y F 2013 *Langmuir* **29** 3097

[14] Han Z Z, Liao L, Wu Y T, Pan H B, Shen S F and Chen J Z 2012 *J. Hazard. Mater.* **217–218** 100

[15] Park S, Kim J S, Yoo K, Lee J C, Anderson W A and Lee J H 2007 *J. Nanosci. Nanotechnol.* **7** 4069

[16] Aal A A, Mahmoud S A and Aboul-Gheit A-K 2009 *Mater. Sci. Eng. C* **29** 831

[17] Baruah S, Jaisai M and Dutta J 2012 *Catal. Sci. Technol.* **2** 918

[18] Mohan R, Krishnamoorthy K and Kim S-J 2012 *Chem. Phys. Lett.* **539–540** 83

[19] Xu F, Yuan Z-Y, Du G-H, Ren T-Z, Bouvy C and Su B-L 2006 *Nanotechnology* **17** 588

[20] Lam S-M, Sin J-C, Abdullah A Z and Mohamed A R 2013 *Mater. Lett.* **93** 423

[21] Bae J, Han J B, Zhang X-M, Wei M, Duan X, Zhang Y and Wang Z L 2009 *J. Phys. Chem. C* **113** 10379

[22] Chu D W, Masuda Y, Ohji T and Kato K 2010 *Langmuir* **26** 2811

[23] Eley C, Li T, Liao F L, Fairclough S M, Smith J M, Smith G and Tsang S C E 2014 *Angew. Chem. Int. Ed.* **53** 7838

[24] Phuruangrat A, Yayapao O, Thongtem T and Thongtem S 2014 *J. Nanomater.* **2014** 367529

[25] Zhang Y Y, Raman M J, Stefanakos E K and Goswami Y 2012 *J. Nanomater.* **2012** 624520

[26] Fan Z Y and Lu J G 2005 *J. Nanosci. Nanotechnol.* **5** 1561

[27] Baruah B and Dutta J 2009 *Sci. Technol. Adv. Mater.* **10** 013001

[28] Mondal C, Sinha A K, Ganguly M, Pal J, Dhara S, Negishi Y and Pal T 2014 *CrystEng Comm* **16** 4322

[29] Wang Y X, Li X Y, Lu G, Quan X and Chen G 2008 *J. Phys. Chem. C* **112** 7332

[30] Damen T C, Porto S P S and Tell B 1966 *Phys. Rev.* **142** 570

[31] Sun Y J, Wang L, Yu X G and Chen K Z 2012 *CrystEngComm* **14** 3199

[32] Yuan J Q, Choo E S G, Tang X S, Sheng Y, Ding J and Xue J M 2010 *Nanotechnology* **21** 185606

[33] Xue X-Y, Chen Z-H, Xing L-L, Ma C-H, Chen Y-J and Wang T-H 2010 *J. Phys. Chem. C* **114** 18607

[34] Hu Q, Tong G X, Wu W H, Liu F T, Qian H S and Hong D Y 2013 *CrystEngComm* **15** 1314

[35] van Dijken A, Meulenkamp E A, Vanmaekelbergh D and Meijerink A 2000 *J. Phys. Chem. B* **104** 1715

[36] Fabbri F, Villani M, Catellani A, Calzolari A, Cicero G, Calestani D, Calestani G, Zappettini A, Dierre B, Sekiguchi T and Salviati G 2014 *Sci. Rep.* **4** 5158

[37] Zhu Q, Xie C S, Li H Y, Yang C Q, Zhang S P and Zeng D W 2014 *J. Mater. Chem. C* **2** 4566

[38] Tam K H, Cheung C K, Leung Y H, Djurišić A B, Ling C C, Beling C D, Fung S, Kwok W M, Chan W K, Phillips D L, Ding L and Ge W K 2006 *J. Phys. Chem. B* **110** 20865

[39] Willander M, Nur O, Sadaf J R, Qadir M I, Zaman S, Zainelabdin A, Bano N and Hussain I 2010 *Materials* **3** 2643

[40] Gong Y Y, Andelman T, Neumark G F, O'Brien S and Kuskovsky I G 2007 *Nanoscale Res. Lett.* **2** 297

[41] Janotti A and Van de Walle C G 2005 *Appl. Phys. Lett.* **87** 122102

[42] Liao Z, Zhang H, Zhou Y, Xu J, Zhang J and Yu D 2008 *Phys. Lett. A* **372** 4505

[43] Vanheusden K, Seager C H, Warren W L, Tallant D R and Voigt J A 1996 *Appl. Phys. Lett.* **68** 403

[44] Ahn C H, Kim Y Y, Kim D C, Mohanta S K and Cho H K 2009 *J. Appl. Phys.* **105** 013502

[45] Wu L L, Wu Y S, Pan X R and Kong F Y 2006 *Opt. Mater.* **28** 418

[46] Wang M S, Zhou Y J, Zhang Y P, Kim E J, Hahn S H and Seong S G 2012 *Appl. Phys. Lett.* **100** 101906

[47] Wang J C, Liu P, Fu X Z, Li Z H, Han W and Wang X X 2009 *Langmuir* **25** 1218

[48] Lin X P, Huang T, Huang F Q, Wang W D and Shi J L 2006 *J. Phys. Chem. B* **110** 24629

[49] Horikoshi S, Saitou A, Hidaka H and Serpone N 2003 *Environ. Sci. Technol.* **37** 5813